


## *In Situ* Quantification of Surface Chemistry in Porous Collagen Biomaterials

DIMITRIOS S. TZERANIS <sup>1,3</sup>, ERIC C. SOLLER,<sup>1</sup> MELISSA C. BUYDASH,<sup>1</sup> PETER T. C. SO,<sup>1,2</sup> and IOANNIS V. YANNAS<sup>1,2</sup>

<sup>1</sup>Department of Mechanical Engineering, Massachusetts Institute of Technology, Cambridge, MA 02139, USA; <sup>2</sup>Department of Biological Engineering, Massachusetts Institute of Technology, Cambridge, MA 02139, USA; and <sup>3</sup>Department of Mechanical Engineering, National Technical University of Athens, 15780 Zografou, Greece

(Received 2 May 2015; accepted 1 September 2015; published online 14 September 2015)

Associate Editor Agata A. Exner oversaw the review of this article.

**Abstract**—Cells inside a 3D matrix (such as tissue extracellular matrix or biomaterials) sense their insoluble environment through specific binding interactions between their adhesion receptors and ligands present on the matrix surface. Despite the critical role of the insoluble matrix in cell regulation, there exist no widely-applicable methods for quantifying the chemical stimuli provided by a matrix to cells. Here, we describe a general-purpose technique for quantifying *in situ* the density of ligands for specific cell adhesion receptors of interest on the surface of a 3D matrix. This paper improves significantly the accuracy of the procedure introduced in a previous publication by detailed marker characterization, optimized staining, and improved data interpretation. The optimized methodology is utilized to quantify the ligands of integrins  $\alpha_1\beta_1$ ,  $\alpha_2\beta_1$  on two kinds of matched porous collagen scaffolds, which are shown to possess significantly different ligand density, and significantly different ability to induce peripheral nerve regeneration *in vivo*. Data support the hypothesis that cell adhesion regulates contractile cell phenotypes, recently shown to be inversely related to organ regeneration. The technique provides a standardized way to quantify the surface chemistry of 3D matrices, and a means for introducing matrix effects in quantitative biological models.

**Keywords**—Adhesion, Biomaterials, Collagen, Extracellular matrix, Integrin, Nerve regeneration, Surface chemistry.

### INTRODUCTION

Cells *in vivo* interact extensively with 3D matrices, such as the native extracellular matrix (ECM) of tis-

sues or implanted biomaterials. Cells sense and respond to their insoluble microenvironment through specific binding interactions between their adhesion receptors and ligands present on the matrix surface. The effects of such cell–matrix interactions have been shown to affect strongly key cell phenotypes. Examples include the role of ECM in tumor progression,<sup>2,23</sup> and the ability of certain biomaterials to induce regeneration,<sup>33</sup> or control stem cell fate.<sup>15</sup>

A prerequisite for cell–matrix interactions is the presence of appropriate ligands for cell adhesion receptors on the matrix. Many studies have focused on the identity of adhesion ligands present on ECM biomolecules, particularly ligands for integrins, the major family of adhesion receptors.<sup>16</sup> In particular, it has been shown that cells bind to collagen type I (the major ECM component of many tissues) mainly *via* collagen-binding integrins, which recognize several ligands on the collagen molecule<sup>6,29</sup>. Although there is significant progress in characterizing elementary binding interactions of adhesion receptors to their ligands on ECM molecules,<sup>24</sup> the chemical environment sensed by cells inside tissue stroma or biomaterial grafts has been not been studied in detail yet.

The surface chemistry of a matrix (defined here as the density of ligands for particular adhesion receptors available to cells) determines which adhesion receptors can be utilized by cells, controls the perception of the cell about its insoluble environment, and induces intracellular signaling.<sup>25</sup> Despite its importance, the vast majority of published studies on cell–matrix interactions do not report the surface chemistry of the utilized matrix. Few studies report instead the mass of

Address correspondence to Dimitrios S. Tzeranis, Department of Mechanical Engineering, National Technical University of Athens, 15780 Zografou, Greece. Electronic mail: tzeranis@gmail.com, tzeranis@mail.ntua.gr

adsorbed matrix biomolecules on cell culture dishes,<sup>10,22,31</sup> a measurement not necessary analogous to its surface chemistry. A key reason for this omission is the lack of appropriate methods for quantifying the surface chemistry of the insoluble microenvironment of cells. The few available methods are often non-quantitative, and not widely-applicable, since they can be applied only in RGD-functionalized synthetic biomaterials.<sup>3,12,19</sup> Some spectroscopic techniques can quantify chemical groups on the surface of biomaterials,<sup>18,20</sup> however these measurements cannot be converted straightforwardly into density of ligands of particular adhesion receptors.

This study describes in detail a technique for quantifying the density of ligands of a particular adhesion receptor on the surface of a 3D matrix *in situ*. It improves significantly the accuracy of the concept introduced in a previous publication<sup>30</sup> in three ways: (1) detailed characterization of fluorescent analogs of the two major collagen-binding integrins ( $\alpha_1\beta_1$ ,  $\alpha_2\beta_1$ ), (2) optimized marker staining protocols that increase sensitivity and minimize background staining, (3) estimation of ligand density *via* a binding model that considers the nature of soluble marker to an 3D matrix. The methodology is utilized to quantify the ligands of integrins  $\alpha_1\beta_1$ ,  $\alpha_2\beta_1$  on two matched porous collagen scaffolds, similar to grafts used clinically in induced peripheral nerve regeneration. The effects of biomaterial surface chemistry were investigated by imaging *ex vivo* sections of transected peripheral nerves treated with the two scaffolds and focusing on the effects of surface chemistry on cell-scaffold adhesion and wound contraction, a phenotype proposed to affect critically the final wound healing outcome.<sup>33</sup>

## MATERIALS AND METHODS

### *Scaffold Fabrication*

Sheets of porous collagen scaffolds were fabricated by freeze-drying a 0.5% w/v micro-fibrillar collagen *I* suspension using published protocols.<sup>27</sup> The dry outcome of freeze-drying (scaffold A) is cross-linked by either dehydro-thermal treatment (DHT) at 120 °C for 48 h at 50 mTorr (scaffold D) or chemically *via* treatment with 14.4 mM EDC and 5.6 mM NHS for 1 h at room temperature (scaffold E), Fig. 1a.

### *Expression and Purification of I Domains*

Soluble fluorescent analogs of the two major collagen-binding integrins ( $\alpha_1\beta_1$ ,  $\alpha_2\beta_1$ ) were prepared by fusing the tetracysteine (TC) tag WDCCPGCKK at the N-terminus of the *I* domains of the  $\alpha$  subunit of the

corresponding integrin by PCR.<sup>1</sup> GST-I domain fusion proteins were expressed in BL21 *e*-coli, purified *via* affinity chromatography, and treated with thrombin to remove the GST domain following published protocols.<sup>6,29</sup> *I* domain solutions were carefully concentrated *via* filter centrifugation in assay buffer (PBS, 2 mM MgCl<sub>2</sub>, 2 mM TCEP, 0.02% tween20), stored at 4°C, and used within 20 days. The concentration and purity of purified *I* domain solutions was evaluated *via* 280 nm absorption and SDS-PAGE.

### *Circular Dichroism Spectroscopy*

The contribution of secondary structures in purified *I* domain solutions was estimated by circular dichroism spectroscopy in an Aviv Model 202 CD spectrometer (Aviv Biomedical) using a far-UV quartz cuvette (New Era enterprises Inc). *I* domain solutions were diluted in assay buffer so that their 280 nm absorption was approximately 0.17. The measured ellipticity  $\theta(\lambda)$  was buffer corrected and converted into mean residue ellipticity  $\theta_{mrw}(\lambda)$ . Secondary structure contribution was estimated by three soft ware tools (SELCON3, CONTINLL, CDSSTR, Colorado State University). For tag-free *I* domains secondary structure predictions were compared with secondary structures annotated in X-ray structures 1QCY and 1AOX.

### *Surface Plasmon Resonance*

The binding of purified recombinant *I* domains to collagen *I* or gelatin was evaluated *via* the surface plasmon resonance (SPR) assay in a BIACORE T100 (GE Healthcare Bio-Sciences AB) following previously published protocols.<sup>6</sup> 1200 RU of ligands (30  $\mu$ g/ml collagen *I* from tail tendon (BD biosciences) or gelatin (collagen *I* denatured by heating at 65 °C for 30') in 10 mM sodium acetate pH 4.5 were immobilized on the surface of CM5 chips (GE Healthcare): collagen *I* in chambers 2 and 4, gelatin in chamber 3, no ligand in chamber 1. The binding of each analyte to its immobilized ligands was studied by flowing 40  $\mu$ L/min solutions of increasing analyte concentration (0.05 to 6  $\mu$ M in HBS-P + supplemented with 1 mM MgCl<sub>2</sub>) for 3 min, followed by dissociation in 40  $\mu$ L/min running buffer for 12 min, and regeneration by 20  $\mu$ L/min regeneration buffer (HBS-P+, 10 mM EDTA, 0.01% v/v SDS) for 1 min. Each condition was performed in duplicates. Raw sensorgrams were processed either by custom-written software (Supplementary Material) or by the BiaEval software (GE Healthcare). Data processing includes compensation of various artifacts, and global fitting of corrected sensorgrams into a 1:1 binding model that describes the kinetics of the detected SPR signal  $R(t)$ :

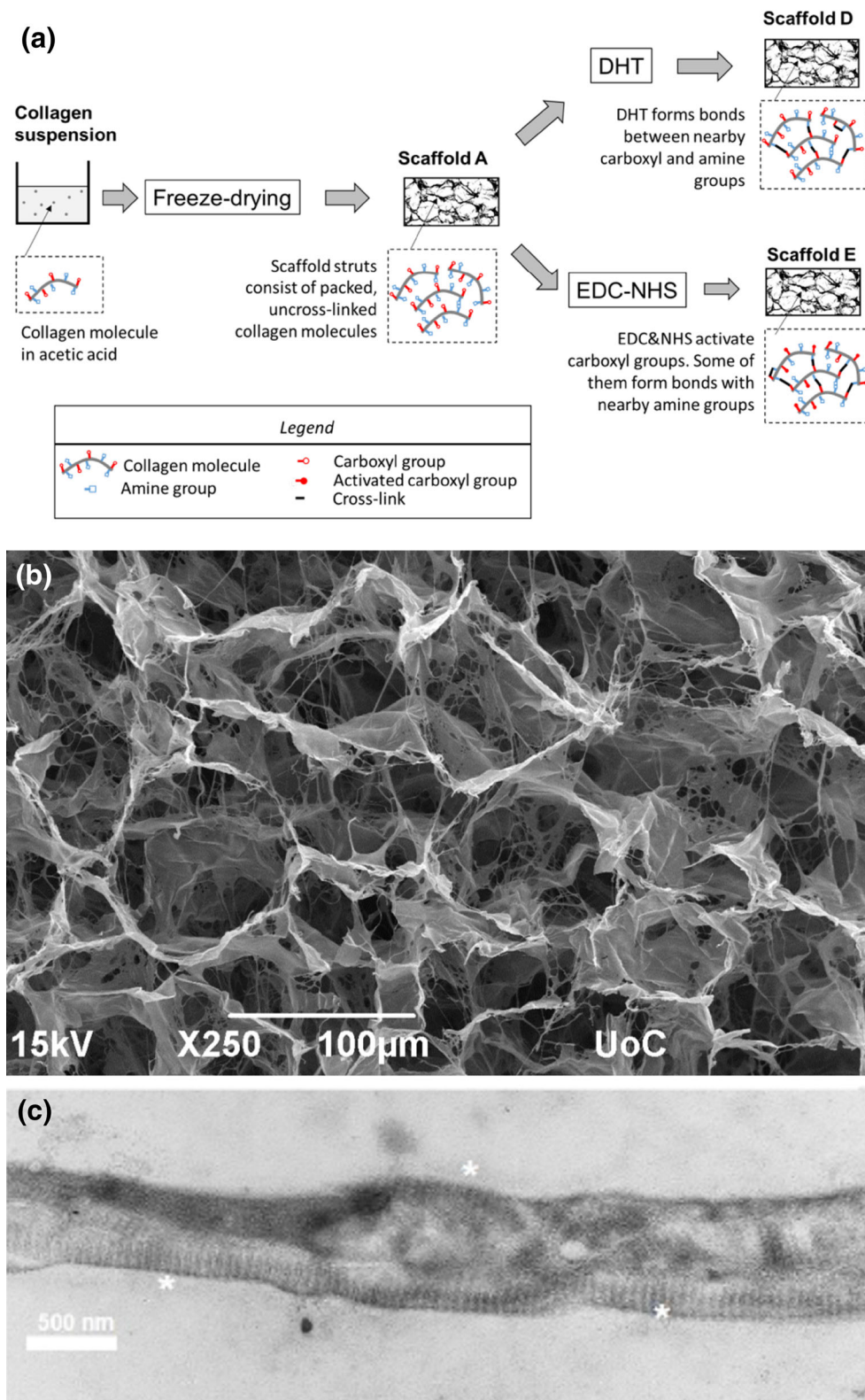


**FIGURE 1.** Structure of porous collagen scaffolds probed in this study. (a) Schematic of scaffold fabrication flow-chart highlighting differences in the chemistry of the two methods utilized for scaffold cross-linking. (b) SEM image of a collagen scaffold highlighting its porous structure and the dimensions of its struts (Image acquired by A. Kourgiantaki, University of Crete). (c) High magnification TEM image of a scaffold strut demonstrating D-banding in microfibrillar collagen (asterisks).



$$\frac{dR}{dt} + (k_{\text{on}} \cdot I_0 + k_{\text{off}}) \cdot R = k_{\text{on}} \cdot I_0 \cdot R_{\text{max}}$$

where  $k_{\text{on}}$  and  $k_{\text{off}}$  are the association and dissociation rates of the analyte-ligand binding reaction,  $I_0$  is analyte concentration,  $M_I$  and  $M_C$  are the MW of  $I$  domain and collagen respectively, and  $R_{\text{max}}$  is the maximum steady state signal achieved when all ligands per collagen molecule are bound to analyte.

#### Ligand Density Assay

Ligand density measurements took place in cylindrical scaffold samples (2 mm diameter, 3 mm height) in PCR tubes. Scaffold samples were hydrated in PBS, blocked with 100  $\mu\text{L}$  superblock in PBS (Thermo scientific) for 3 h at 4  $^{\circ}\text{C}$ , treated with stained TC-tagged  $I$  domain solutions (sometimes supplemented with non-tagged  $I$  domains) overnight at 4  $^{\circ}\text{C}$ , and imaged in a multi-photon microscope (Fig. 3a). Each binding assay consists of two distinct experiments. In “binding” experiments,  $I$  domain buffer is supplemented with 2 mM  $\text{MgCl}_2$ . In “control” experiments,  $I$  domain buffer is supplemented with 10 mM EDTA. TC-tagged  $I$  domain staining is done by treatment with 1 mM TCEP for 2 h at 4  $^{\circ}\text{C}$  and then with 5% excess FIAsh-EDT<sub>2</sub> in the presence of 1 mM  $\beta\text{me}$  and 1 mM TCEP for 3 h at 4  $^{\circ}\text{C}$ . Careful removal of unbound FIAsh from FIAsh-stained  $I$  domains *via* gel filtration (micro bio-spin 6, Biorad Laboratories Inc.) prevents non-specific binding of FIAsh to blocking agents bound on the matrix, which causes background fluorescence and induces experimental noise. Removal of unbound FIAsh also eliminates the need for a BAL wash, a step included in the initial procedure<sup>30</sup> that reduces accuracy (BAL affects specific binding of FIAsh to TC-tagged  $I$  domains).

3D images of scaffolds on glass-bottom dish treated with fluorescently-labeled  $I$  domains were acquired by a spectral multi-photon microscope.<sup>5</sup> Imaging parameters: image planes are located 10 to 30  $\mu\text{m}$  away from the scaffold surface, 4.8 mW laser power, 775 nm laser wavelength, 40  $\mu\text{s}$  pixel acquisition time, 256  $\times$  256 pixels, 0.21  $\mu\text{m}$  pixel size, Zeiss C-apochromat 40  $\times$  1.2 NA water immersion objective lens. For each experiment two z-stacks are acquired per sample. After spectral unmixing and image segmentation, ligand density measurements are based on the FIAsh emission of pixels located at the outer surface of scaffold struts (Supplementary Material). This emission is converted into equivalent FIAsh concentration using a standard curve. In contrast to the earlier preliminary publication where ligand density was expressed in units of ligands/ $\mu\text{m}^2$ <sup>30</sup> here the density of ligands is

expressed in Molar units since new experimental data showed that  $I$  domains can slowly diffuse and bind ligands inside the whole scaffold strut volume.

#### Binding Model

The estimation of adhesion ligand density  $L_0$  is based on a 1:1 binding model that describes the binding of soluble  $I$  domains to their immobilized ligands present in the 3D matrix. In this case it can be shown (Supplementary Material) that  $L_0$  (in units of M) can be estimated as:

$$L_0 = 4 \cdot k_D \cdot \left. \frac{dB_{ss}}{dI_0} \right|_{I_0=k_D}$$

where  $B_{ss}(I_0)$  is the measured concentration of  $I$  domains bound on a matrix when the matrix is treated with an  $I$  domain solution of concentration  $I_0$ . The slope  $\frac{dB_{ss}}{dI_0}$  is estimated from binding assay data.  $k_D = k_{\text{off}}/k_{\text{on}}$  is the dissociation constant of  $I$  domain binding to collagen, estimated from BIACORE data.

#### Animal Experiments

NIH guidelines (85-23 Rev. 1985) were observed for all surgical procedures.<sup>27</sup> Adult female Lewis rats were anesthetized, the sciatic nerve was anesthetized topically and transected. The nerve stumps were inserted into the ends of a collagen conduit, leaving a 15 mm gap between the nerve stumps. The gap is then filled with saline, and the scaffold is secured using nylon sutures. Animals were sacrificed 1 or 9 weeks post-injury by CO<sub>2</sub> inhalation. The excised tissue was fixed in 4% paraformaldehyde in on ice for 8 h, immersed in 30% sucrose solution overnight, immersed in Optimal Cutting Temperature medium, flash frozen in liquid nitrogen, cryo-sectioned at 10  $\mu\text{m}$  thickness on a microtome, and stored at  $-20^{\circ}\text{C}$ . Sections were later thawed at room temperature for 30 min, washed twice in TBST for 10 min, blocked and permeabilized in blocking solution (Dako) supplemented with 0.3% Triton X100 for 1 h at room temperature, treated with AlexaFluor488-conjugated wheat germ agglutinin (Life Technologies) overnight at 4  $^{\circ}\text{C}$ , washed twice in PBS for 10 min, counterstained with 10 ng/ml DAPI and 1:100 rhodamine-phalloidin (Life Technologies), and coverslipped.

Low-magnification images of labeled sections were acquired in an Olympus IX81 fluorescence microscope equipped with an ORCA CCD detector (Hamamatsu, Japan) using a Fluor 4 $\times$  objective lens. High-magnification images were acquired by a spectral multi-photon microscope.<sup>5</sup> Imaging parameters: 8 mW laser power, 775 nm laser wavelength, 40  $\mu\text{s}$  pixel acquisition

tion time, 0.21  $\mu\text{m}$  pixel size. The signal contributions of emission sources was resolved by spectral unmixing.

## RESULTS

The methodology developed for quantifying the density of ligands for a particular adhesion receptor on a 3D matrix consists of three steps: (1) Development of soluble fluorescent analogs (markers) of each adhesion receptor of interest *via* genetic engineering. In contrast to antibodies which recognize single epitopes that are not necessarily related to adhesion ligands, such fluorescent analogs bind to all ligands of the corresponding receptor with similar affinity as the receptor of interest. (2) Conduct a series of binding assays of the markers on the 3D matrix, where the density of fluorescent markers bound on their ligands on the matrix is quantified by 3D microscopy, and (3) Estimate the density of adhesion ligands on the matrix by fitting the binding assay data to an appropriate binding model.

The technique is demonstrated by quantifying the density of adhesion ligands for the two major collagen-binding integrins ( $\alpha_1\beta_1$ ,  $\alpha_2\beta_1$ ) in two kinds of matched porous collagen scaffolds. These biomaterials were chosen because they recently showed remarkably different ability to induce regeneration in a standardized animal model of peripheral nerve (PN) injury 9 weeks post-injury.<sup>27</sup> Scaffold D is similar to the FDA-approved devices Integra<sup>TM</sup> and Neuragen<sup>TM</sup>, which are applied clinically in patients with severe burns and limb paralysis respectively.<sup>4,11</sup> Scaffolds D and E have identical pore geometry and chemical composition (they are fabricated using the same protocol), Fig. 1a, but differ in the final cross-linking treatment. Scaffold D has been cross-linked by dehydro-thermal treatment (DHT). Scaffold E has been cross-linked chemically by EDAC and NHS. As baseline reference, scaffold A was the outcome of freeze-drying without cross-linking.

For each integrin of interest ( $\alpha_1\beta_1$ ,  $\alpha_2\beta_1$ ) two kinds of soluble markers were expressed, and affinity purified: the non-fluorescent marker (the *I* domain of integrin  $\alpha_i$  subunit), and the same *I* domain tagged with a tetracysteine (TC) motif. The *I* domain of the  $\alpha$  subunit of a collagen-binding integrin recognizes and binds to the same adhesion ligand as does the corresponding integrin.<sup>6,16,29</sup> When the TC tag binds the biarsenical dye FAsH, the complex becomes fluorescent,<sup>1</sup> generating soluble fluorescent markers of the ligands of the corresponding integrin. The TC-FAsH system was preferred over fusing *I* domains to a fluorescent protein, due to its small size (1 kDa) that was expected to affect the conformation-sensitive binding affinity of *I* domains much less.<sup>1</sup> SDS-PAGE stained by FAsH reveals that only TC-tagged *I*

domains become fluorescent upon FAsH treatment (Fig. 2a).

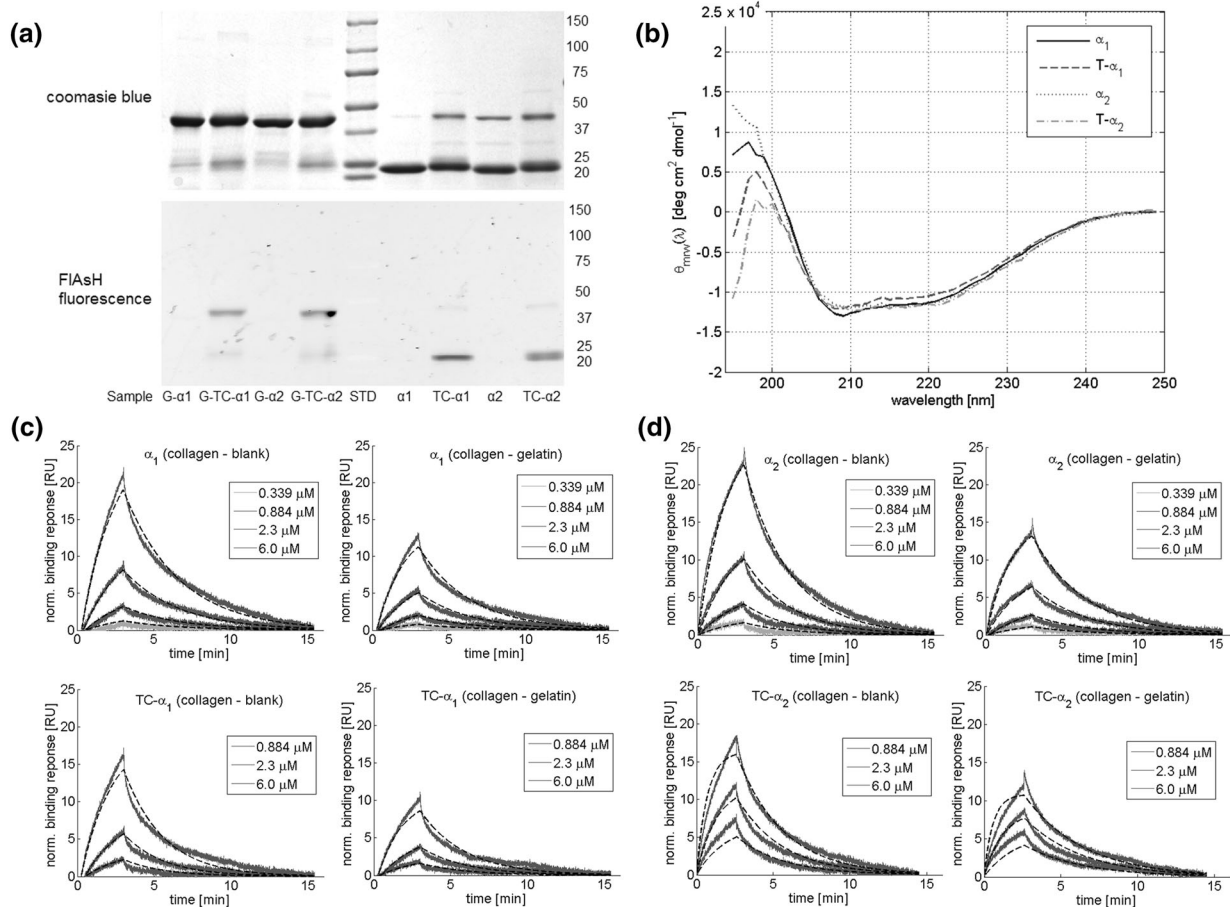
The properties of purified *I* domains were evaluated *via* circular dichroism (CD) spectroscopy, and surface plasmon resonance analysis of their binding to collagen (BIAcore assay). Predictions of secondary structure based on CD data suggest that the TC tag slightly decreases the contribution of  $\alpha$ -helices and  $\beta$ -sheets and increases the contribution of turns and random coil, in agreement with the published hairpin structure of the TC tag.<sup>21</sup> Adding the TC tag affects acquired CD spectra  $\theta_{mrv}(\lambda)$  mostly below 200 nm (Fig. 2b). CD analysis tools provide similar predictions of secondary structure contribution (Table S1). Estimated contributions for tag-free *I* domains agree well with the secondary structure annotated in published X-ray structures. Fitting BIAcore binding data (Figs. 2c and 2d) to first-order binding equations suggested that the dissociation constants for  $\alpha_1$  and  $\alpha_2$  *I* domain binding to collagen *I* were 8.45  $\mu\text{M}$  and 9.10  $\mu\text{M}$  respectively (Table S2). BIAcore data show that binding of native non-tagged *I* domains (denoted as  $\alpha_i$ , where  $i = 1, 2$ ) and TC-tagged *I* domains (denoted as TC- $\alpha_i$ ,  $i = 1, 2$ ) to collagen have similar kinetics (TC tag causes small  $k_D$  increase) and magnitude. Finally, both native *I* domains and TC-tagged *I* domains bind to collagen significantly more than gelatin (Figs. 2c and 2d), in agreement with the known dependence of integrin-collagen binding on collagen conformation.<sup>9,29</sup>

The density of adhesion ligands for each receptor of interest and in each scaffold type was estimated based on a series of *in situ* binding experiments. Samples of collagen scaffolds were blocked and treated with solutions of fluorescent markers of increasing concentration in the absence or presence of non-fluorescent markers. Binding experiments took place in the presence of either 2 mM  $\text{Mg}^{+2}$  (“signal” experiments) or 10 mM EDTA (“control” experiments). After overnight incubation in fluorescent marker solution, biomaterials were imaged in a spectral multi-photon microscope (Fig. 3a). The detected images contain the emission of both collagen and FAsH, which were separated by spectral unmixing (Fig. 3b). Results show that FAsH emission in the presence of 10 mM EDTA was always much lower compared to the emission in the presence of 2 mM  $\text{MgCl}_2$  (Fig. 3b). The effect of  $\text{Mg}^{+2}$  on TC-tagged *I* domain binding to its ligands on collagen agrees with the published divalent cation-dependent mechanism of integrin-ligand binding and has been reported in previous studies of *I* domain binding to collagen.<sup>6,29</sup> Compared to the preliminary data presented in a previous publication,<sup>30</sup> the optimized staining protocol utilized here resulted in 4 $\times$  higher FAsH emission with minimal background signal

(Fig. 3b). The density of fluorescent markers that bind specifically onto ligands on the scaffold was estimated by subtracting the FIAsH emission of “control” experiments from the emission of “signal” experiments (Fig. 4a). Increasing the concentration of non-fluorescent markers in the presence of constant concentration of fluorescent markers reduced the density of fluorescent markers bound on the scaffold, suggesting saturable specific binding of *I* domains on the scaffold (Fig. 4b). Adhesion ligand density was estimated by globally fitting data from a series of binding experiments into a binding model that describes binding of soluble *I* domains to immobilized ligands on a 3D scaffold. Data fitting provided estimates of  $204.9 \pm 41 \mu\text{M}$   $\alpha_1\beta_1$  ligands and  $248.3 \pm 61 \mu\text{M}$   $\alpha_2\beta_1$  ligands in scaffold D ( $n = 3$ ),  $29.4 \pm 7.2 \mu\text{M}$   $\alpha_1\beta_1$  li-

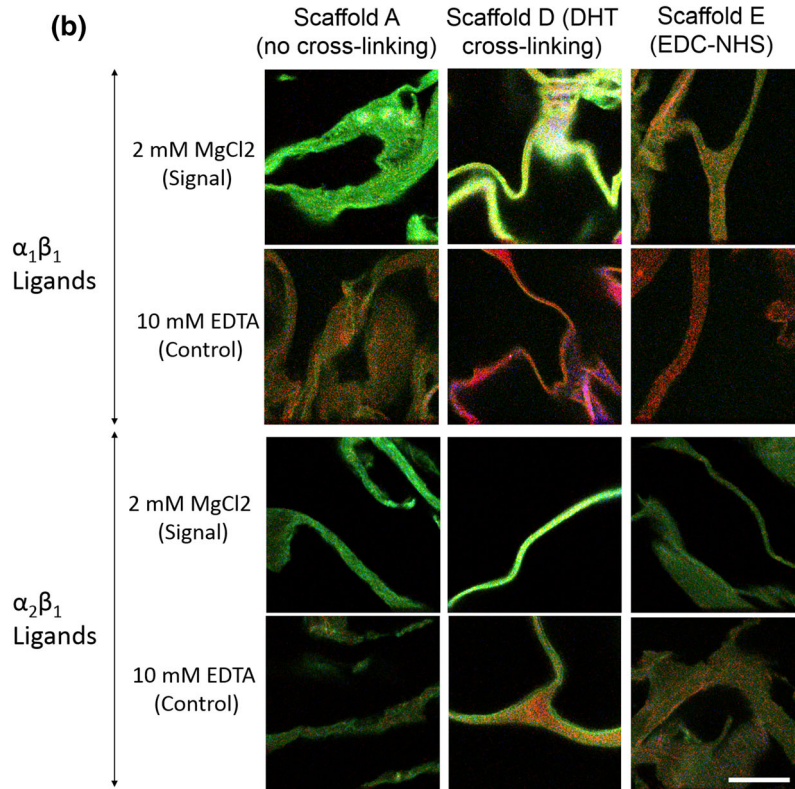
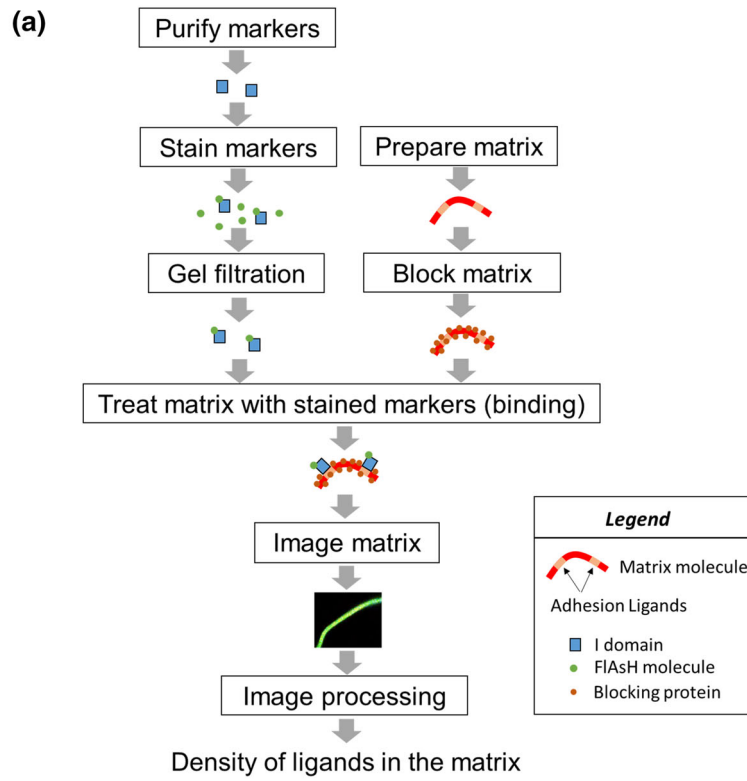
**FIGURE 3. Optical-based ligand density quantification in 3D matrices using fluorescent analogs of adhesion receptors. (a) Schematic of the procedure for quantifying the density of adhesion ligands on a 3D matrix (b) Representative data of the imaging-based binding assay utilized for quantifying the surface chemistry of a matrix *in situ*. 16-channel spectral data shown after the separation of collagen and FIAsH emission by spectral unmixing. Data display scaffold struts (detected by the collagen autofluorescence) in the red channel and FIAsH emission (from labeled TC-tagged *I* domains bound to collagen ligands) in the green channel. Scaffold samples have been treated with either  $6 \mu\text{M}$  fluorescently labeled TC- $\alpha_1$  (rows 1, 2) or  $6 \mu\text{M}$  YC- $\alpha_2$  (rows 3–4) in the presence of  $2 \text{ mM}$   $\text{MgCl}_2$  (“signal” experiments, rows 1 and 3) or  $10 \text{ mM}$  EDTA (“control” experiments, rows 2 and 4). Bar:  $20 \mu\text{m}$ .**

gands and  $75.6 \pm 11.0 \mu\text{M}$   $\alpha_2\beta_1$  ligands in scaffold E ( $n = 3$ ), and  $148.2 \pm 26.3 \mu\text{M}$   $\alpha_1\beta_1$  ligands and  $214.3 \pm 50.1 \mu\text{M}$   $\alpha_2\beta_1$  ligands in scaffold A ( $n = 3$ )



**FIGURE 2. Biochemical characterization of the purified *I* domains and TC-tagged *I* domains. (a) SDS-FIAsH-PAGE analysis of purified fractions of non-tagged and TC-tagged *I* domains before and after thrombin cleavage. Samples were reduced by TCEP and stained by FIAsH before denaturing and loading.<sup>1</sup> After electrophoresis, the gel was imaged first in a fluorescent imager (bottom), and then it was stained using coomassie blue and imaged in a conventional imager (top). STD: protein standards. Results highlight that only TC-tagged *I* domains become fluorescent upon FIAsH treatment (b) Circular dichroism spectra of purified *I* domain solutions. (c, d) Corrected sensorgrams (solid lines) and global fits (dashed lines) to a 1:1 binding model for analyte solutions of *I* domains of integrin  $\alpha_1$  (c) and integrin  $\alpha_2$  (d). Top row: Results for solutions of non-tagged *I* domains. Bottom row: Results for solutions of TC-tagged *I* domains. Left Column: Signal corresponding to *I* domain binding to a collagen surface minus the signal of *I* domain binding to a gelatin surface. Right Column: Signal corresponding to *I* domain binding to a collagen surface minus the signal of *I* domain binding to a gelatin surface.**





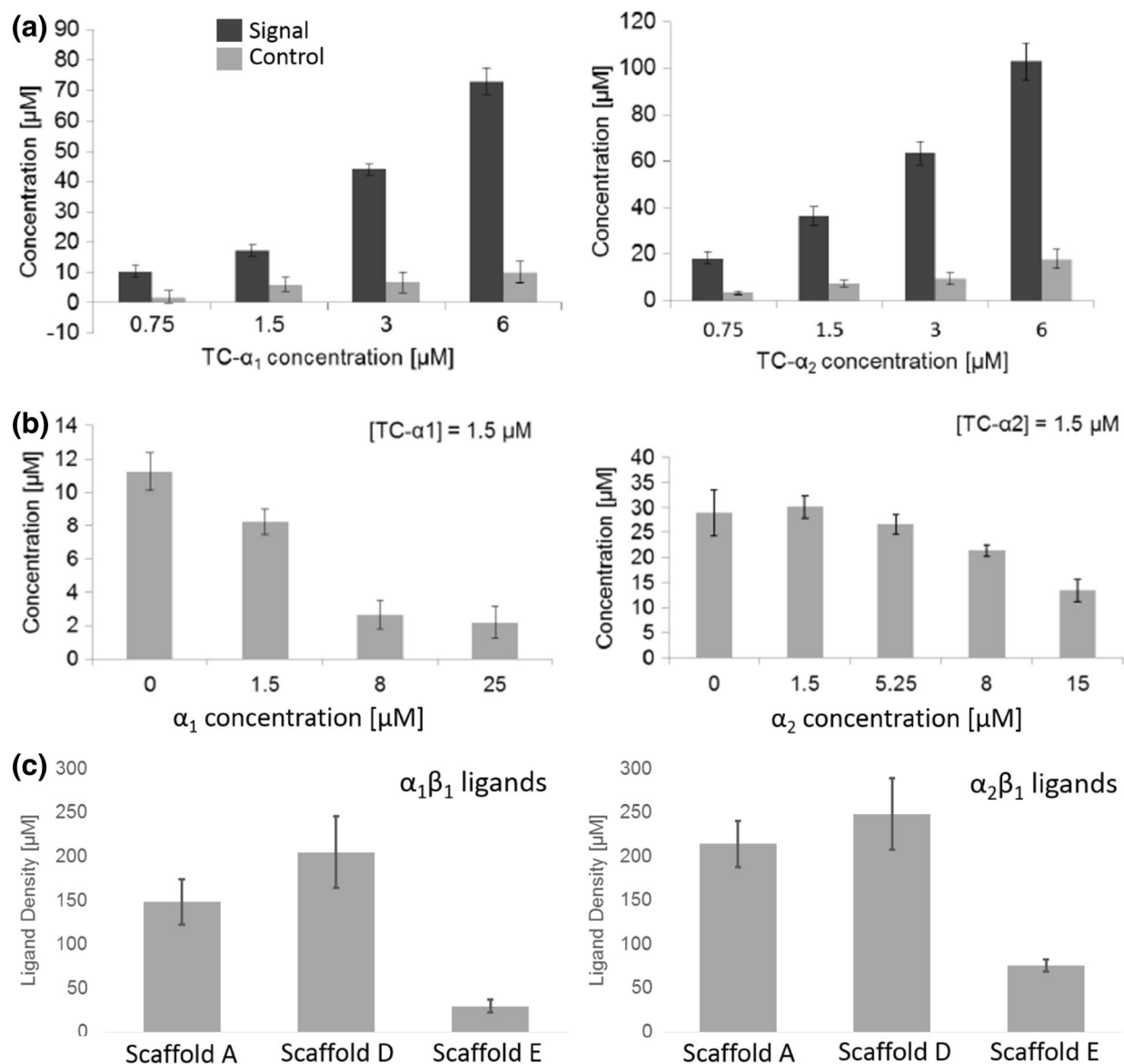


**FIGURE 4.** Quantifying the surface chemistry of porous collagen scaffolds *in situ*. (a) Equivalent concentration of fluorescent *I* domains bound on scaffold D as a function of fluorescent marker concentration and the presence of  $\text{Mg}^{2+}$ . (b) Competitive binding of 1.5  $\mu\text{M}$  fluorescent *I* domains on scaffold D in the presence of increasing concentrations of non-fluorescent *I* domains. (c) Estimated concentrations of ligands of integrin  $\alpha_1\beta_1$  (left), and  $\alpha_2\beta_1$  (right) in scaffolds D, E and the baseline scaffold A demonstrate that scaffold D contains significantly more ligands of  $\alpha_1\beta_1$  and  $\alpha_2\beta_1$  than scaffold E. A pairwise *t* test suggests that the density of  $\alpha_1\beta_1$  or  $\alpha_2\beta_1$  ligands in scaffolds D and E are significantly different ( $p = 0.047$  and  $p = 0.101$ ,  $n = 3$ , respectively). A pairwise *t* test suggests that the density of  $\alpha_1\beta_1$  or  $\alpha_2\beta_1$  ligands in scaffolds D and A are not significantly different ( $p = 0.319$  and  $p = 0.690$ ,  $n = 3$ , respectively).

(Fig. 4c). These data showed that EDAC-NHS cross-linking reacts with and effectively destroys  $\alpha_1\beta_1$ ,  $\alpha_2\beta_1$  ligands in scaffold E, in agreement with the known chemical mechanism of EDAC (attacks carboxyl groups), and the presence of carboxyl groups in key acidic residues of  $\alpha_1\beta_1$ ,  $\alpha_2\beta_1$  ligands.<sup>24</sup> On the other hand, DHT cross-linking appeared not to affect the surface chemistry of the scaffolds since the measured ligand density of scaffolds D and A were not significantly different.

The importance of the surface chemistry of a 3D matrix is demonstrated by quantifying its effects in the application of collagen scaffolds in PN regeneration. It has been shown that certain porous collagen scaffolds can induce regeneration in skin and PN, and that this regenerative ability depends strongly on specific scaffold features.<sup>27,34</sup> The underlying molecular details of this dependence are not known yet. Experimental data from skin<sup>34</sup> and PN regeneration<sup>27</sup> and recent observations in African mice that spontaneously regenerate



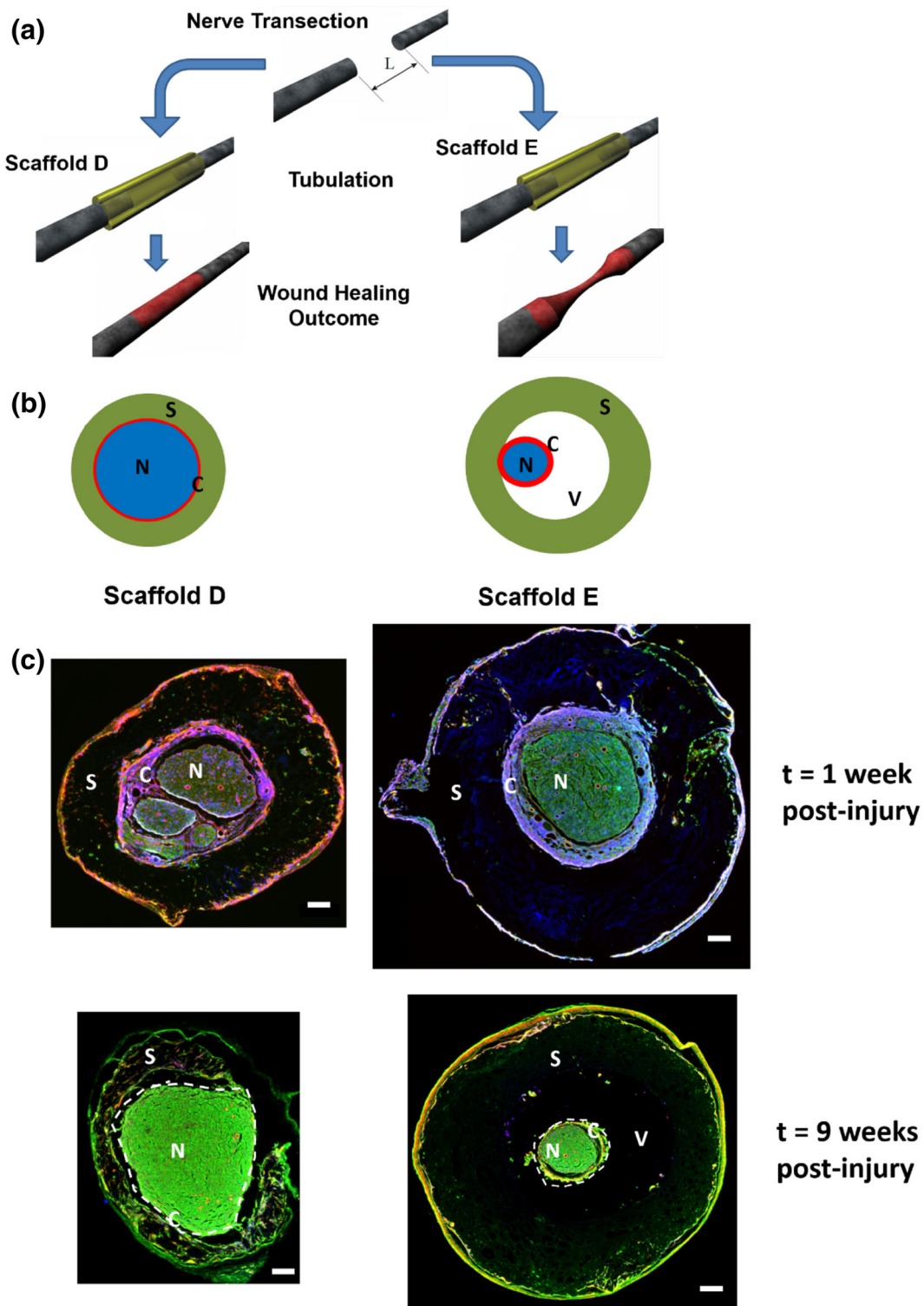


**FIGURE 5.** Tubular collagen scaffolds of different surface chemistry grafted in transected peripheral nerves interact differently with contractile cells that cause wound contraction. (a) Schematic of the rat sciatic nerve transection model. (b) Schematic of the morphology observed in cross-sections of harvested nerves from animal groups D (left) or E (right) 9 weeks post-injury. A capsule of contractile cells (C; red) forms between newly-formed nerve tissue (N; blue) and scaffold (S; green). In group E a large void volume (V) forms between the capsule and the scaffold's inner lumen. (c) Fluorescent images of nerve cross sections, harvested 1 (top row) or 9 weeks post injury (bottom row). Sections were stained for actin (phalloidin; red), cell content (Wheat Germ Agglutinin; green) and nuclei (DAPI; blue). Nerve trunks are highlighted by a white dashed line. Bars: 200  $\mu\text{m}$ .

their skin<sup>26</sup> suggest that regenerative activity correlates with down-regulation of wound contraction. The requirement for cells to adhere to their surrounding matrix in order to apply significant contractile forces suggests that the surface chemistry of a biomaterial may affect its regenerative activity *via* regulating wound contraction. In order to get evidence that could support this hypothesis, a follow-up study of the previous 9-week animal study,<sup>27</sup> was designed: rat sciatic nerves were transected, the resulting stumps were separated by 15 mm, inserted in tubular collagen scaffolds D or E (Fig. 5a) and harvested 1 or 9 weeks post-injury. The 9 week time point serves as an indicator of the final wound healing outcome.<sup>7</sup> The 1 week time point provides evidence about the effects of the biomaterial during the critical early wound healing response.<sup>32</sup>

Low magnification images of PN regenerates harvested 1 or 9 weeks post-injury (Figs. 5b and 5c) show an assembly of contractile cells (capsule) that surrounds the newly formed nerve tissue (regenerate). The mechanical forces applied by capsule cells are the origin of macroscopic wound contraction.<sup>33</sup> The diameter and number of axons that manage to cross half the gap 9 weeks post-injury have been proposed as quality metrics of the wound healing outcome. The nerve regenerate in animal group D had a significantly larger diameter compared to animal group E both 1 and 9 weeks post-injury, in agreement with its increased regenerative activity.<sup>27</sup> Furthermore, regenerates in animal group D were surrounded by a significantly thinner capsule compared to group E ( $82.9 \pm 8.6 \mu\text{m}$  vs.  $158.0 \pm 31.3 \mu\text{m}$  1 week post-injury,  $31 \pm 5 \mu\text{m}$  vs.  $73 \pm 18 \mu\text{m}$  9 weeks post-injury,  $n = 3$ ), a sign of reduced wound contraction (Figs. 5b and 5c). In both animal groups, the contractile cell capsule (highlighted as “C”) has already filled the volume between the regenerate and the scaffold as soon as 1 week post-injury, suggesting fast kinetics of wound contraction that could potentially have significant effects in the delicate fibrin bridge that connects the two nerve stumps during the early phase of wound healing.<sup>32</sup>

Low magnification images suggest two possible ways that scaffold surface-chemistry that could affect the wound healing outcome. First, they show that capsule cells have different extent of contact with the surrounding scaffold. In group D capsule cells make firm contact with the surrounding scaffold both at 1 and 9 weeks post-injury around the whole perimeter of the regenerate (Figs. 5b and 5c left). On the other hand, during cryo-sectioning of samples from animal group E there were frequent artifacts (tears) in the capsule-scaffold interface, in agreement with the hypothesis that capsule cells are not strongly attached to the surrounding scaffold E. 9 weeks post-injury in

animal group E the capsule and the scaffold are usually separated by void volume suggesting loss of contact or poor cell-scaffold adhesion (Figs. 5b and 5c right). Second, the extent of cell migration inside the two kinds of scaffolds is very different. In group D a significantly larger number of cells infiltrates inside the scaffold both at 1 and 9 weeks post-injury compared to group E (Fig. 5c), suggesting that cells cannot migrate inside scaffold E despite the fact that is made of collagen I.

High-magnification multi-photon imaging was then utilized to zoom in the same cross sections and study in detail the region where capsule cells bind to the collagen scaffold. High magnification images show that the capsule consists of circumferentially-oriented collagen fibers (visualized *via* the second harmonic emission of tissue collagen) and actin-rich contractile cells (Fig. 6). The different extent of cell-scaffold interactions is again evident. In group D contractile cells in the outer layer of the capsule bound extensively on the scaffold inner lumen and their long axis intersected with the scaffold outline, indicating that cells transmit forces to the scaffold (Fig. 6 left). By contrast, in group E capsule cells in the outer capsule layer stain strongly for actin, were much more elongated (both signs of increased contractility), and their long axes were strongly aligned in the circumferential direction. These observations suggest that in animal group E capsule cells apply forces to each other rather than to the surrounding scaffold. The strictly circumferential orientation and high cell aspect ratio is observed in animal group E both at 1 and 9 weeks post-injury and is independent on whether the capsule is in contact with the surrounding inner lumen of the scaffold (Fig. 6 right).

High resolution imaging also reveals that in group D, many individual cells managed to migrate inside the scaffold (as soon as 1 week post-injury) and bind to its struts in a spindle-like shape. These cells are contractile (stain brightly for actin) and synthesize new collagen fibers, which are detected based on their bright second harmonic emission (Fig. 6 bottom left). On the other hand, in animal group E the scaffold area in the proximity of its inner lumen lacks any infiltrating cells (Fig. 6 bottom right).

## DISCUSSION

This work presents a novel technique for quantifying the surface chemistry of an insoluble 3D matrix, such as tissue ECM or a biomaterial. The technique fulfills the critical need to quantify and compare the chemical stimuli provided to cells by various insoluble microenvironments. It provides a direct description of

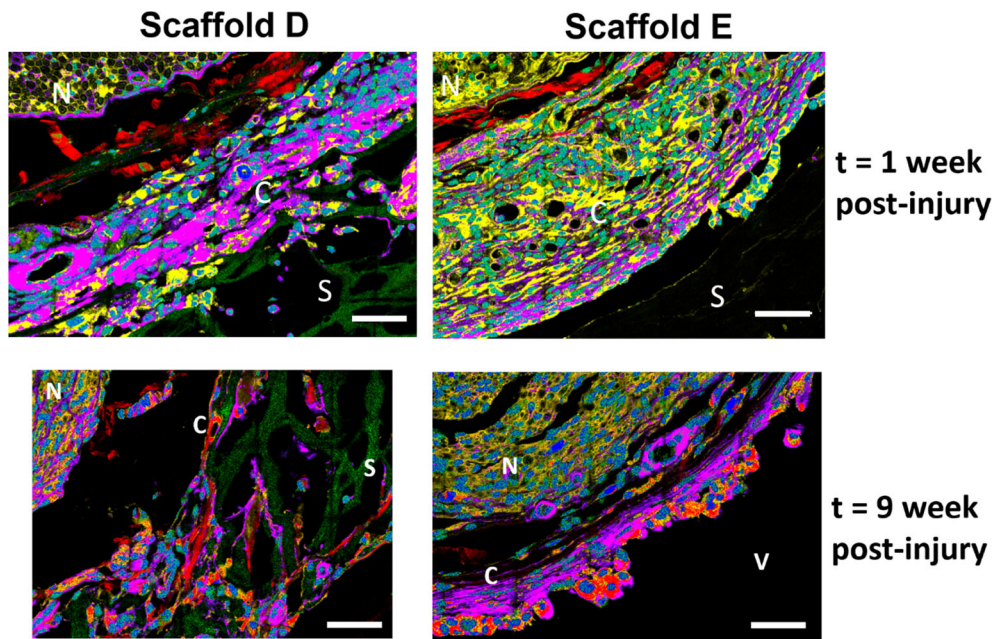


**FIGURE 6.** High-magnification multi-photon images of *ex vivo* nerve cross sections highlight differences in the cell binding pattern to collagen scaffolds of different surface chemistry. All images are zoom-ins of the fluorescent images shown in Fig. 5, acquired in the bottom right corner of nerve tissue. Nerve cross sections were grafted with scaffolds D (left column) or E (right column) and harvested 1 week (top row) or 9 weeks (bottom row) post injury. Images are shown after spectral unmixing displaying the key sources of emission in the samples: WGA (yellow), phalloidin (purple), DAPI (blue), collagen autofluorescence (green) and second harmonic emission (red). Bars: 50  $\mu\text{m}$ .

the chemical microenvironment perceived by cells, in contrast to measurements of average macroscopic properties (e.g. chemical composition) that are not entities directly sensed by cells.

While several studies have focused on the molecular interactions between cell adhesion receptors and ECM molecules *in vitro*,<sup>6,29</sup> it has not been so far possible to quantify the extent of these interactions in the native 3D insoluble microenvironment where cells actually interact with these molecules. It is expected that the magnitude of chemical stimuli provided by a matrix to cells depends on its chemical composition, component cross-linking, chemical treatments, nanoscale topology and spatial arrangement of matrix molecules in 3D space.<sup>18,22,28</sup>

Here, the technique utilizes TC-tagged *I* domains as fluorescent analogs of collagen-binding integrins. *I* domains have been extensively utilized to study integrin binding to collagens.<sup>6,21,29</sup> Although most studies focus on *I* domain binding to tropocollagen, collagen *I* in tissues always forms super-molecular structures such as fibrils and fibers. A related study revealed that fibril formation reduced the affinity of *I* domains to collagen.<sup>17</sup> This study goes a step further, and utilizes fluorescent *I* domains to quantify *in situ* for the first time the surface chemistry of two matched scaffolds made of microfibrillar collagen *I* (the fibril nature of collagen causes the D-banding shown in Fig. 1c).

Biochemical characterization of purified *I* domains overall suggest that the addition of the TC tag makes *I*

domains fluorescent without significantly disturbing their secondary structure and binding characteristics to collagen (Fig. 2, Tables S1, S2). Data show that  $\alpha_2$  was affected more by the addition of the TC tag compared to  $\alpha_1$ . Optimized FIASH staining of TC-tagged *I* domains improved significantly the sensitivity and accuracy of the method compared to the preliminary procedure<sup>30</sup> and provided the sensitivity required to discriminate 3D matrices of different surface chemistry. Results show that scaffold D (cross-linked by DHT) provides to cells  $204.9 \pm 41 \mu\text{M}$   $\alpha_1\beta_1$  and  $248.3 \pm 61 \mu\text{M}$   $\alpha_2\beta_1$  ligands. This is approximately one order of magnitude higher compared to the density of ligands provided by scaffold E (cross-linked by EDC and NHS) and not significantly different compared to the density of ligands provided by the uncross-linked scaffold. These results highlight a significant effect of the cross-linking method on biomaterial surface chemistry.

Although the results presented focus on ligands of integrins  $\alpha_1\beta_1$ ,  $\alpha_2\beta_1$  on porous collagen scaffolds, the methodology can be extended to quantify the ligands for different types of adhesion receptors in different kinds of cell-free matrices such as biomaterials, physiologic vs. pathologic tissue ECM, or decellularized tissues. Prerequisites for such extensions are the development of appropriate fluorescent analogs of the adhesion receptor of interest, and the utilization of an appropriate binding model that can describe the nature of marker binding on the matrix under investigation.



Ligand density measurements can help clarify how 3D matrices modulate key cell phenotypes that affect biological processes. First, the significantly more extensive cell adhesion (adhesion of capsule cells to the scaffold inner lumen, adhesion of cells to scaffold struts as they migrate inside the scaffold) to scaffold D compared to scaffold E (Figs. 5, 6) could result by the increased ligand density of scaffold D (Fig. 4). This dramatic effect in cell-scaffold adhesion cannot be explained by differences in other material properties, specifically the sevenfold increased stiffness,<sup>13</sup> and the increased *in vivo* degradation rate of scaffold E compared to scaffold D.<sup>14</sup> In addition, the contractile cell capsule morphology observed 9-weeks post-injury in animal group E resembles the one observed in transected PN grafted with silicone tubes,<sup>8</sup> materials that lack adhesion ligands, suggesting that this similarity can be explained by a paucity of adhesion ligands in scaffold E. We speculate that the limited ability of cells to bind scaffold E could lead cells to instead interact more with their surrounding cells and could possibly explain why in animal group E a thicker capsule consisting of multiple concentric layers of contractile cells forms within 1 week.

The combined observations of Figs. 4, 5, and 6 also agree with a simple mechanism that has been proposed to partly explain how biomaterials regulate the wound healing outcome.<sup>33</sup> This mechanism suggests that regeneration is impeded by the effects of mechanical stress fields in the wound, induced by cell forces in the contractile cell capsule. In the case of PN, elementary cell forces in the capsule sum up along the circumferential axis (hoop stresses) causing compression of the enclosed nerve tissue, which was shown to correlate inversely with the quality of the wound healing outcome.<sup>27</sup>

Finally, the new technique offers a way for bringing materials science closer to quantitative biology. So far, any chemical stimuli provided by the surrounding matrix to cells have been described in a qualitative manner. By providing a standardized quantification of the chemical stimuli provided by a matrix to cells, the new method enables the incorporation of matrix effects in quantitative systems-level models of signal transduction. Efforts in this area have so far neglected to account for signal transduction effects of the surrounding matrix.

#### ELECTRONIC SUPPLEMENTARY MATERIAL

The online version of this article (doi: [10.1007/s10439-015-1445-x](https://doi.org/10.1007/s10439-015-1445-x)) contains supplementary material, which is available to authorized users.

#### ACKNOWLEDGMENTS

The cDNA of  $I$  domains ( $\alpha 1$ ,  $\alpha 2$ ) of integrin subunits  $\alpha 1$  and  $\alpha 2$  were a kind gift of Sue Craig (Martin Humphries Lab, University of Manchester, UK). We thank Dr. Amit Roy for performing the initial protein expressions and purifications, Mrs Debby Pheasant (MIT biophysical instrumentation facility) for valuable technical assistance in the circular dichroism experiments, Dr. Albert Tai (genomics facility core, Tufts University) for valuable technical assistance in the BIACORE experiments, and Prof. K. Van Vliet for providing access to the fluorescent microscope of her lab. The authors acknowledge financial support from the National Institutes of Health grant RO1 NS051320 (I.V.Y., D.S.T., E.C.S., P.T.C.S.), the Biomechanics Training Grant T32EB006348 (E.C.S.), the National Science Foundation Graduate Research Fellowship DGE-1122374 (M.C.B), Singapore Alliance for Science and Technology Center, BioSym IRG and Singapore and MIT Alliance 2, CSB program (P.T.C.S., and D.S.T.), and National Institutes of Health grant 9P41EB015871-26A1 (P.T.C.S.).

#### REFERENCES

- Adams, S. R., R. E. Campbell, L. A. Gross, B. R. Martin, G. K. Walkup, Y. Yao, J. Llopis, and R. Y. Tsien. New Biarsenical Ligands and Tetracysteine Motifs for Protein Labeling In Vitro and In Vivo: Synthesis and Biological Applications. *J. Am. Chem. Society* 124:6063-6076, 2002.
- Allen, M., and J. L. Jones. Jekyll and Hyde: the role of the microenvironment on the progression of cancer. *J. Pathol.* 223:162-176, 2011.
- Barber, T. A., G. M. Harbers, S. Park, M. Gilbert, and K. E. Healy. Ligand density characterization of peptide-modified biomaterials. *Biomaterials* 26:6897-6905, 2005.
- Boeckstyns, M. E., A. I. Sørensen, J. F. Viñeta, B. Rosén, X. Navarro, S. J. Archibald, J. Valls-Solé, M. Moldovan, and C. Krarup. Collagen conduit versus microsurgical neuroorrhaphy: 2-year follow-up of a prospective, blinded clinical and electrophysiological multicenter randomized, controlled trial. *J Hand Surg Am.* 38:2405-2411, 2013.
- Buehler, C., K. H. Kim, U. Greuter, N. Schlumpf, and P. T. So. Single-photon counting multicolor multiphoton fluorescence microscope. *J Fluoresc.* 15: 41-51, 2005.
- Calderwood, D. A., D. S. Tuckwell, J. Eble, K. Kühn, and M. J. Humphries. The integrin  $\alpha 1 A$ -domain is a ligand binding site for collagens and laminin. *J. Biol. Chem.* 272:12311-12317, 1997.
- Chamberlain, L. J., I. V. Yannas, H. P. Hsu, G. Strichartz, and M. Spector. Collagen GAG substrate enhances the quality of nerve regeneration through collagen tubes up to level of autograft. *Exp Neurol* 154:315-329, 1998.
- Chamberlain, L. J., I. V. Yannas, H. P. Hsu, and M. Spector. Connective tissue response to tubular implants for peripheral nerve regeneration: the role of myofibroblasts. *J Comp Neurol.* 417:415-430, 2000.



- <sup>9</sup>Emsley, J., C. G. Knight, R. W. Farndale, M. J. Barnes, and R. C. Liddington. Structural basis of collagen recognition by integrin  $\alpha 2\beta 1$ . *Cell* 101:47-56, 2000.
- <sup>10</sup>Engler, A., L. Bacakova, C. Newman, A. Hategan, M. Griffin, and D. Discher. Substrate compliance versus ligand density in cell on gel responses. *Biophys J.* 86:617-628, 2004.
- <sup>11</sup>Graham, G. P., S. D. Helmer, J. M. Haan, and A. Khandelwal. The use of Integra® Dermal Regeneration Template in the reconstruction of traumatic degloving injuries. *J Burn Care Res.* 34:261-266, 2013.
- <sup>12</sup>Harbers, G. M., L. J. Gamble, E. F. Irwin, D. G. Castner, and K. E. Healy. Development and characterization of a high-throughput system for assessing cell-surface receptor-ligand engagement. *Langmuir* 21:8374-8384, 2005.
- <sup>13</sup>Harley, B. A., Leung, J. H., Silva, E. C., and Gibson, L. J. Mechanical characterization of collagen-glycosaminoglycan scaffolds. *Acta Biomater.* 3:463-74, 2007.
- <sup>14</sup>Harley, B. A., Spilker, M. H., Wu, J. W., Asano, K., Hsu, H. P., Spector, M., and Yannas I. V. Optimal degradation rate for collagen chambers used for regeneration of peripheral nerves over long gaps. *Cells Tissues Organs* 176:153-65, 2004.
- <sup>15</sup>Huebsch, N., P. R. Arany, A. S. Mao, D. Shvartsman, O. A. Ali, S. A. Bencherif, J. Rivera-Feliciano, and D. J. Mooney. Harnessing traction-mediated manipulation of the cell/matrix interface to control stem-cell fate. *Nat Mater.* 9:518-526, 2010.
- <sup>16</sup>Hynes, R. O. Integrins: bidirectional, Allosteric Signaling Machines. *Cell* 110:673-687, 2002.
- <sup>17</sup>Jokinen, J., E. Dadu, P. Nykvist, J. Käpylä, D. J. White, J. Ivaska, P. Vehviläinen, H. Reunanen, H. Larjava, L. Häkkinen, and J. Heino. Integrin-mediated cell adhesion to type I collagen fibrils. *J Biol Chem.* 279:31956-31963, 2004.
- <sup>18</sup>Kingshott, P., G. Andersson, S. L. McArthur, and H. J. Griesser. Surface modification and chemical surface analysis of biomaterials. *Curr Opin Chem Biol.* 15:667-676, 2011.
- <sup>19</sup>Kong, H. J., T. Boonthekul, and D. J. Mooney. Quantifying the relation between adhesion ligand-receptor bond formation and cell phenotype. *Proc Natl Acad Sci U.S.A.* 103:18534-18539, 2006.
- <sup>20</sup>Ma, Z., Z. Mao, and C. Gao. Surface modification and property analysis of biomedical polymers used for tissue engineering. *Colloids Surf B Biointerfaces* 60:137-157, 2007.
- <sup>21</sup>Madani, F., J. Lind, P. Damberg, S. R. Adams, R. Y. Tsien, and A. O. Gräslund. Hairpin structure of a biarsenical-tetracysteine motif determined by NMR spectroscopy. *J Am Chem Soc.* 131:4613-4615, 2009.
- <sup>22</sup>Maheshwari, G., G. Brown, D. A. Lauffenburger, A. Wells, and L. G. Griffith. Cell adhesion and motility depend on nanoscale RGD clustering. *J Cell Sci.* 113:1677-1686, 2000.
- <sup>23</sup>Naba, A., K. R. Clauser, S. Hoersch, H. Liu, S. A. Carr, and R. O. Hynes. The matrisome: in silico definition and in vivo characterization by proteomics of normal and tumor extracellular matrices. *Mol Cell Proteomics* 11:M111.014647, 2012.
- <sup>24</sup>Plow, E. F., T. A. Haas, L. Zhang, J. Loftus, and J. W. Smith. Ligand binding to integrins. *J Biol Chem.* 275:21785-21788, 2000.
- <sup>25</sup>Schiller, H. B., C. C. Friedel, C. Boulegue, and R. Faessler. Quantitative proteomics of the integrin adhesome show a myosin II-dependent recruitment of LIM domain proteins. *EMBO Rep.* 12:259-266, 2011.
- <sup>26</sup>Seifert, A. W., S. G. Kiama, M. G. Seifert, J. R. Goheen, T. M. Palmer, and M. Maden. Skin shedding and tissue regeneration in African spiny mice (*Acomys*). *Nature* 489:561-565, 2012.
- <sup>27</sup>Soller, E. C., D. S. Tzeranis, K. Miu, P. T. So, and I. V. Yannas. Common features of optimal collagen scaffolds that disrupt wound contraction and enhance regeneration both in peripheral nerves and in skin. *Biomaterials* 33:4783-4791, 2012.
- <sup>28</sup>Sweeney, S. M., J. P. Orgel, A. Fertala, J. D. McAuliffe, K. R. Turner, G. A. Di Lullo, S. Chen, O. Antipova, S. Perumal, L. Ala-Kokko, A. Forlino, W. A. Cabral, A. M. Barnes, J. C. Marini, and J. D. San Antonio. Candidate cell and matrix interaction domains on the collagen fibril, the predominant protein of vertebrates. *J Biol Chem.* 283:21187-21197, 2008.
- <sup>29</sup>Tuckwell, D., D. A. Calderwood, L. J. Green, and M. J. Humphries. Integrin  $\alpha 2$  I-domain is a binding site for collagens. *J Cell Sci.* 108:1629-1637, 1995.
- <sup>30</sup>Tzeranis, D. S., A. Roy, P. T. So, and I. V. Yannas. An optical method to quantify the density of ligands for cell adhesion receptors in three-dimensional matrices. *J R Soc Interface.* 6:S649-S661, 2010.
- <sup>31</sup>Valenick, L. V., and J. E. Schwarzbauer. Ligand density and integrin repertoire regulate cellular response to LPA. *Matrix Biol.* 25:223-231, 2006.
- <sup>32</sup>Williams, L. R., F. M. Longo, H. C. Powell, G. Lundborg, and S. Varon. Spatial-temporal progress of peripheral nerve regeneration within a silicone chamber: parameters for a bioassay. *J Comp Neurol.* 218:460-470, 1983.
- <sup>33</sup>Yannas, I. V. *Tissue and organ regeneration in adults*. Second edition. New York; Springer, 2015.
- <sup>34</sup>Yannas, I. V., E. Lee, D. P. Orgill, E. M. Skrabut, and G. F. Murphy. Synthesis and Characterization of a model extracellular-matrix that induces partial regeneration of adult mammalian skin. *Proc Natl Acad Sci U.S.A.* 86:933-937, 1989.